DUAL-CHANNEL MORE FLEXIBLE SALAMO-LIKE CHEMOSENSOR FOR FLUOROGENIC SENSING OF COPPER ION IN SEMI-AQUEOUS MEDIUM**

R.-Y. Li [1], S.-X. Gao [2], Ch. Liu [1], W.-K. Dong [1*], Y.-J. Ding [3*]

[1] School of Chemical and Biological Engineering at Lanzhou Jiaotong University, Lanzhou, Gansu, China; e-mail: dongwk@126.com
[2] School of Environmental and Municipal Engineering at Lanzhou Jiaotong University, Lanzhou, Gansu, China
[3] College of Biochemical Engineering at Anhui Polytechnic University, Wuhu, Anhui, China; e-mail: dyj@ahpu.edu.cn

The optical properties of the symmetric salamo-like chemical probe (H_2CS) of Cu^{2+} were studied in EtOH/H_2O (1:1, V/V) solution by UV-Vis and fluorescence spectroscopy. In the fluorescence spectrum, the coordination of Cu^{2+} with H_2CS results in fluorescence quenching owing to the paramagnetic nature of Cu^{2+} ions. The binding constant of Cu^{2+} to the H_2CS sensor was calculated as 1.17×10^{11} M^{-1} and LOD was obtained as 5.3×10^{-8} M. When Cu^{2+} ions were added, the UV-Vis spectra changed, obviously due to the electron transfer from sensor to metal bond, and a new absorption band appeared at 372 nm. When the ethylenediaminetetraacetic acid (EDTA) solution was added to the H_2CS-Cu^{2+} solution, causing a large binding constant, with EDTA releasing the free sensor molecule and finally achieving a fluorescence shutdown phenomenon.

Keywords: *salamo-like probe, chemosensor, synthesis, two-channel detection, ethylenediaminetetraacetic acid reversibility.*

ДВУХКАНАЛЬНЫЙ ГИБКИЙ ХЕМОСЕНСОР ДЛЯ ФЛУОРОГЕННОГО ОПРЕДЕЛЕНИЯ ИОНА МЕДИ В ПОЛУВОДНОЙ СРЕДЕ

R.-Y. Li [1], S.-X. Gao [2], Ch. Liu [1], W.-K. Dong [1*], Y.-J. Ding [3*]

УДК 535.372

[1] Школа химической и биологической инженерии Университета Ланьчжоу Цзяотун, Ланьчжоу, Ганьсу, Китай; e-mail: dongwk@126.com
[2] Школа экологического и муниципального проектирования Университета Ланьчжоу Цзяотун, Ланьчжоу, Ганьсу, Китай
[3] Колледж биохимической инженерии Аньхойского политехнического университета, Аньхой, Китай; e-mail: dyj@ahpu.edu.cn

(Поступила 30 ноября 2020)

С использованием УФ-видимой и флуоресцентной спектроскопии изучены оптические свойства симметричного саламоподобного химического зонда (H_2CS) Cu^{2+} в растворе EtOH/H_2O (1:1, об./об.). Координация Cu^{2+} и H_2CS приводит к затуханию флуоресценции из-за парамагнитной природы ионов Cu^{2+}. Константа связывания Cu^{2+} с сенсором H_2CS $1.17\cdot10^{11}$ M^{-1}, предел обнаружения $5.3\cdot10^{-8}$ М. При добавлении ионов Cu^{2+} УФ-видимые спектры изменяются, очевидно, из-за переноса электронов от сенсора на металлическую связь, появляется новая полоса поглощения при 372 нм. При добавлении раствора этилендиаминтетрауксусной кислоты (ЭДТА) к раствору H_2CS-Cu^{2+} константа связывания с ЭДТА возрастает, что приводит к высвобождению свободной молекулы сенсора и достижению затухания флуоресценции.

**Full text is published in JAS V. 89, No. 1 (http://springer.com/journal/10812) and in electronic version of ZhPS V. 89, No. 1 (http://www.elibrary.ru/title_about.asp?id=7318; sales@elibrary.ru).

Ключевые слова: *саламоподобный зонд, хемосенсор, синтез, двухканальное обнаружение, обратимость этилендиаминтетрауксусной кислоты.*

Introduction. Copper exists in various substances in nature and as an important metal element is widely used in metal wires and coins and so on [1–6]. In recent years, because of its low cost, copper has been widely used as agricultural fungicide, algaecide, insecticide, and nutrient for plant growth [7–12]. In the biological system, a trace smack of Cu^{2+} is an active component of tyrosinase, ceruloplasmin, and superoxide dismutase involved in several key metabolic processes in the nervous system and plays a crucial role in aerobic respiration [13–16]. Nevertheless, as a heavy metal, excessive Cu^{2+} has a significant impact on human health. It can cause Menkes disease, cardiovascular disease, and colon cancer [17–23]. Recently, some new research has revealed that a considerable amount of Cu^{2+} gets into the environment from waste water, and waste residue damages the environment, as well as human health. At present, several methods have been reported for the determination of Cu^{2+} ion, including reverse phase liquid chromatography coupled with electrochemical detection, mass spectroscopy, X-ray fluorescence spectrometry, charge separation, atomic absorption spectroscopy (AAS), and others [24–30]. However, these detection methods usually require complex technology, expensive instruments, and time-consuming procedures, which limit their wide applications in production and daily life. Therefore, it is very important to explore a rapid and convenient detection method for Cu^{2+} ion. Chemical sensors have been widely used in the detection of various metal ions in recent years due to their low cost, simplicity, and high efficiency [31–37]. We report a single salamo-like [31] H_2CS probe, which could be used for dual channel recognition of Cu^{2+} in aqueous solution.

Experimental. All reagents and chemicals were of available analytical reagent grade and can be used without further purification. Aqueous solutions were prepared using double distilled deionized water. Element analyses were obtained on a GmbH VarioEL V3.00 automatic elemental analysis instrument. Melting points were obtained using a microscopic melting point apparatus made in Beijing Taike Instrument Limited Company and were uncorrected. ^{1}HNMR and ^{13}CNMR spectra were determined by a German Bruker AVANCE DRX-400 spectrophotometer. UV-Vis absorption and fluorescence spectra were recorded on Shimadzu UV-2550 and Perkin-Elmer LS-55 spectrometers, respectively.

Synthesis of H_2CS. The synthetic route to the single salamo-like the H_2CS sensor is shown in Fig. 1.

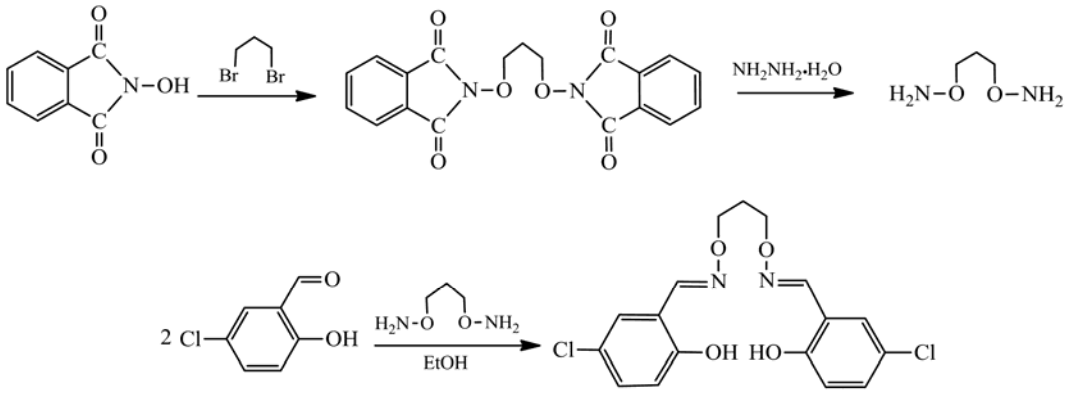

Fig. 1. Synthetic route to the H_2CS sensor.

This H_2CS sensor was synthesized by the methods reported earlier [38]. Yield: 75.8%. m.p.: 164–166°C. Anal. Calcd for $C_{17}H_{16}C_{l2}N_2O_4$ (%): C, 53.28; H, 4.21; N, 7.31. Found: C, 53.45; H, 4.06; N, 7.18. ^{1}HNMR (400 MHz, $CDCl_3$), δ 2.14 (t, J = 6.0 Hz, 2H, CH_2), 4.31 (t, J = 6.0 Hz ,4H, CH_2), 6.85 (d, J = 8.0 Hz, 2H, ArH), 7.25 (s, 2H, ArH), 7.33 (d, J = 8.0 Hz, 2H, ArH), 8.09 (s, 2H, CH=N), 9.80 (s, 2H, OH).

Fluorescence and UV-Vis measurements. The H_2CS sensor was dissolved in EtOH to a final concentration of 1×10^{-5} M; then $Cu(NO_3)_2$ was dissolved in water to a concentration of 1×10^{-3} M. Solutions of other metal ions are prepared in a similar manner. Fluorescence and UV-Vis measurements were performed at room temperature in a 1 cm quartz colorimetric dish. At the same time, any change in the fluorescence intensity was monitored by a fluorescence spectrometer (λ_{ex} = 324 nm with a slit width of 5/10 nm).

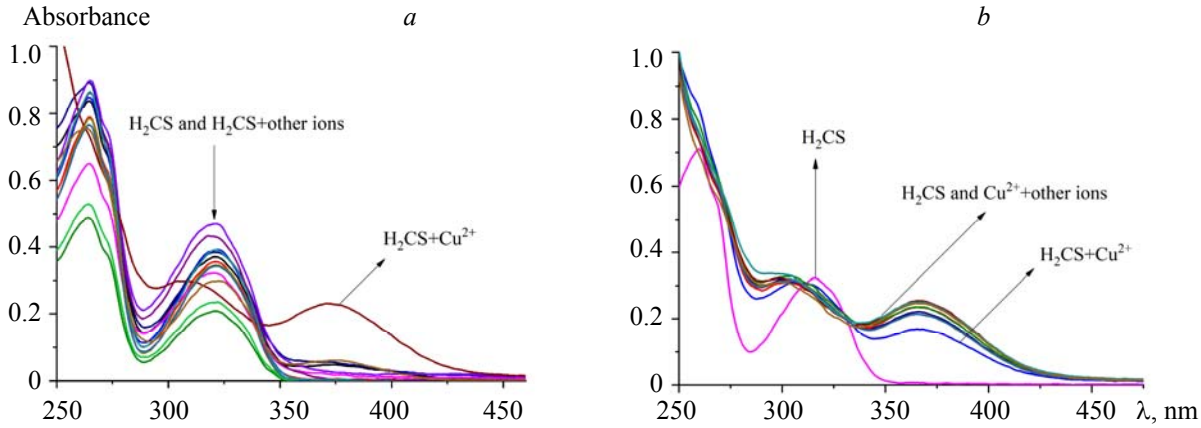

Fig. 2. a) UV-Vis spectra of the H_2CS probe (10^{-5} M, EtOH) recorded after the addition of various metal ions (10^{-3} M, H_2O); b) the competitive experiment for the identification of Cu^{2+} in the presence of other metal ions.

Results and discussion. In order to evaluate the selectivity absorption of the H_2CS probe towards different metal ions (Li^+, Na^+, K^+, Mg^{2+}, Ca^{2+}, Ba^{2+}, Cu^{2+}, Co^{2+}, Ni^{2+}, Zn^{2+}, Cd^{2+}, Pb^{2+}, Hg^{2+}, Cr^{3+}, Al^{3+}, and Ag^+), they were investigated under the same conditions. While adding other metal ions, there were no significant spectral changes except Cu^{2+}, which showed fluorescence quenching effects (Fig. 2a). The absorption peak of the H_2CS sensor at 321 nm showed a blue shift to 305 nm, and a new absorption band appeared at 372 nm, owing to the interaction of Cu^{2+} with H_2CS. The electron transition from Cu^{2+} to the H_2CS probe leads to the MLCT effect. In order to test and verify the practicability of the H_2CS probe, a competitive experiment has been carried out through adding Cu^{2+}, which shows that the other metal ions have no influences on the recognition of Cu^{2+} by H_2CS (Fig. 2b).

The ultraviolet titration experiment of different concentrations of Cu^{2+} ions in ethanol solution was conducted (Fig. 3). A new ultraviolet absorption peak was observed at 321 nm, which was the characteristic absorption peak of salamo-like compounds. With a gradual increase in Cu^{2+} ion concentration, a new absorption peak appeared at approximately 371 nm. When 1 equiv. Cu^{2+} ion was added, there was no change in the UV spectrum, indicating that the titration endpoint had been reached. It can be seen that the liganding of Cu^{2+} ions with N_2O_2 donor disrupts the hydrogen bond in the H_2CS molecule, reduces the conjugation of the system, and changes the ultraviolet-visible spectra [39–43]. In our previous reports, we have obtained a Cu^{2+}

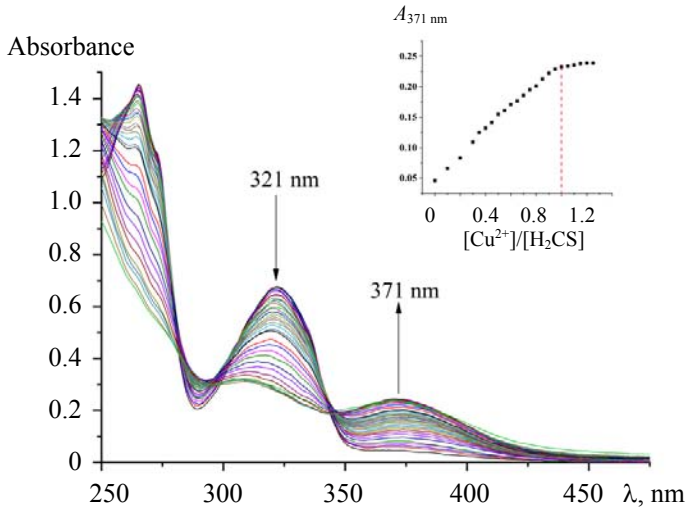

Fig. 3. Ultraviolet titration curves of the H_2CS probe with different concentrations of Cu^{2+} (EtOH/H_2O = 1:1, v/v). Inset: The absorbance at 371 nm varies with the interaction of $[Cu^{2+}]/[H_2CS]$, $[Cu^{2+}] = 10^{-3}$ M, $[H_2CS] = 10^{-5}$ M.

complex of the H_2CS sensor, as shown in Fig. 4. Under the catalysis of Cu^{2+} ions, two C–C and two N–O bonds in H_2CS were fractured and a new complex $[Cu(L^1)_2]$ was obtained. Therefore, we have proved that 1 mol Cu^{2+} ions participate in coordination [44–48].

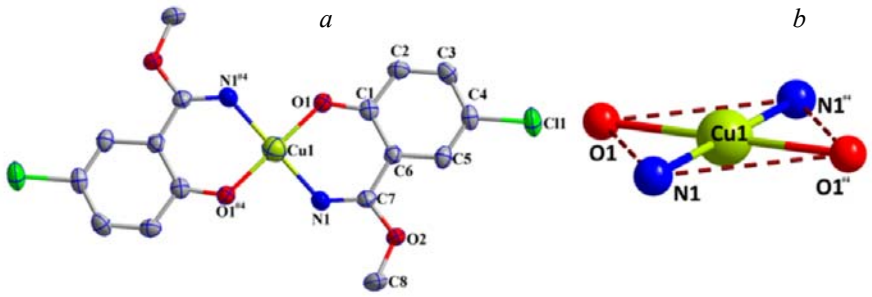

Fig. 4. a) Coordination modes of Cu^{2+} and H_2CS; b) coordination polyhedron for Cu(II) atom.

Fluorescence spectra. The fluorescence spectra of the H_2CS sensor were studied in the presence of various cations (Li^+, Na^+, K^+, Mg^{2+}, Ca^{2+}, Ba^{2+}, Cr^{3+}, Mn^{2+}, Co^{2+}, Ni^{2+}, Cu^{2+}, Zn^{2+}, Cd^{2+}, Al^{3+}, Pb^{2+}, Ag^+, and Pd^{2+}). In order to prove the specificity of the probe for recognition, more organic ions were added. The H_2CS sensor has a strong absorption peak at 347 nm, and at the same time, when other metal ions are added, the absorption peak appears blue when shifted from 380 nm to 374 nm with a new absorption peak appeared at 461 nm [49–51]. However, when Cu^{2+} ions were added, the fluorescence spectra appeared significantly quenched from various cations. The fluorescence profiles at 461 nm of the stoichiometric ratio showed an apparent selectivity for Cu^{2+} ions over other cations in EtOH/H_2O (1:1, v/v) solution (Fig. 5). Due to the Cu^{2+} ion not only having a single electron in its 3d orbit but having a paramagnetic property, the coordination of Cu^{2+} and H_2CS leads to fluorescence quenching phenomenon.

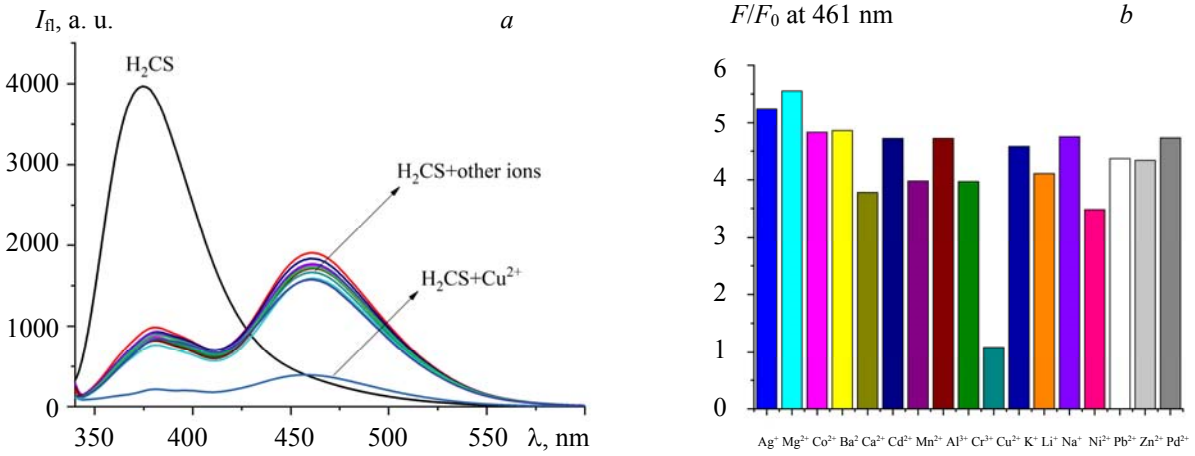

Fig. 5. a) Fluorescence emission spectra of the H_2CS sensor (5×10^{-5} m) in the presence of ions Li^+, Na^+, K^+, Mg^{2+}, Ca^{2+}, Ba^{2+}, Cr^{3+}, Mn^{2+}, Co^{2+}, Ni^{2+}, Cu^{2+}, Zn^{2+}, Cd^{2+}, Al^{3+}, Pb^{2+}, Ag^+, and Pd^{2+} with 1 mL concentration of 1×10^{-3} M, λ_{ex} = 324 nm; b) Its relative fluorescence intensities at 461 nm.

To know more about the properties of Cu^{2+} ions recognized by the H_2CS sensor, a fluorescence anti-interference experiment of the H_2CS sensor was carried out to recognize Cu^{2+} ion. Firstly, by adding 1 mL Cu^{2+} ion aqueous solution to 1 mL H_2CS ethanol solution, the fluorescence is obviously quenched (Fig. 6). Then 0.5 mL Cu^{2+} ion solution was added to 1 ml H_2CS ethanol solution. Subsequently, 0.5 mL aqueous solutions of different metal cations were added respectively. These results reflect the truth that the presence of other metal ions has no influence on the recognition of Cu^{2+} ions.

Because of the fluorescence quenching caused by the coordination, we determined the coordination ratio of the H_2CS sensor and Cu^{2+} ions through the fluorescence titration experiment. The fluorescence spectra of the H_2CS chemosensor in ethanol solution change when different concentrations of Cu^{2+} ions are added

(Fig. 7). When Cu^{2+} ions were added gradually, the fluorescence intensity of H_2CS was visibly quenched [43, 44]. The stoichiometric ratio between Cu^{2+} and H_2CS was 1:1, which is shown in the fluorescence titration experiment. The fluorescence titration experiments were linearly matched to obtain the fitted curves (Fig. 8).

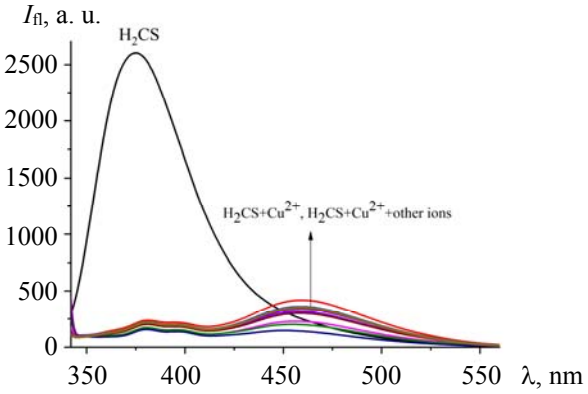

Fig. 6. The fluorescence spectrum of anti-interference experiment of Cu^{2+} ion recognized by the H_2CS sensor in $EtOH/H_2O$ solution, λ_{ex} = 324 nm.

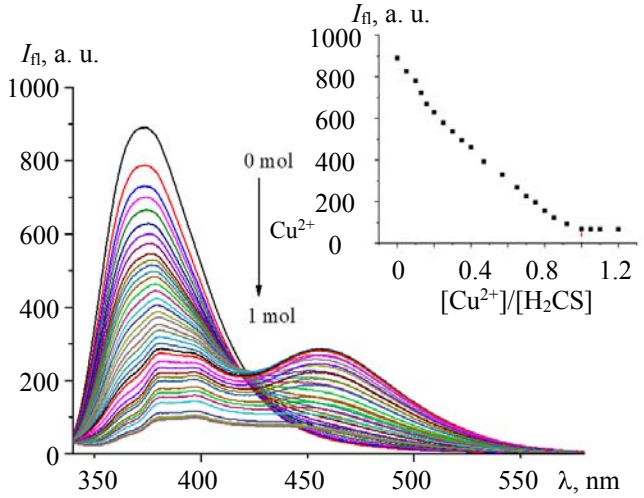

Fig. 7. Fluorescence intensity change of the H_2CS sensor after titration with Cu^{2+} in $EtOH/H_2O$ solution, λ_{ex} = 324 nm. Inset: the fluorescence intensity at 374 nm varies with the interaction of $[Cu^{2+}]/[H_2CS]$.

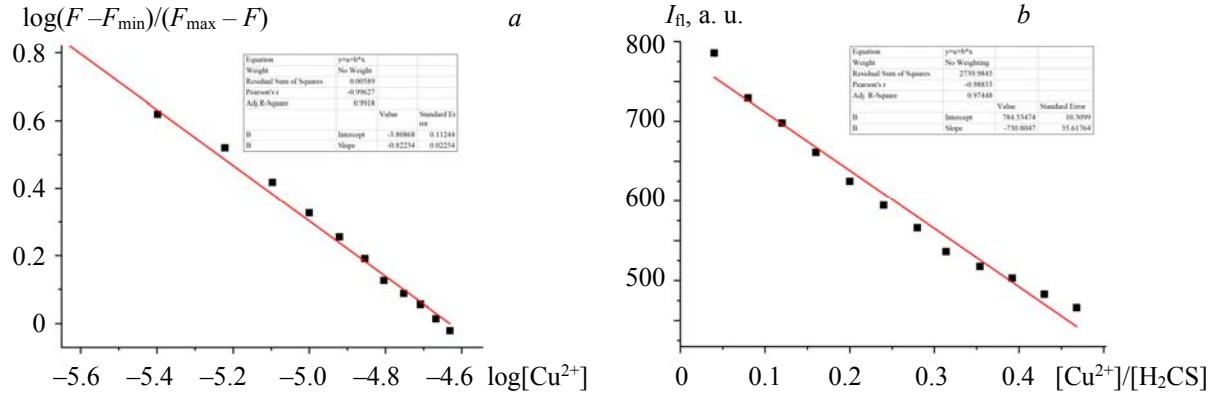

Fig. 8. a) Linear fitting of the H_2CS sensor to Cu^{2+} binding constant; b) plot of fluorescence intensity at 324 nm as a function of $[Cu^{2+}]/[H_2CS]$ molar ratio.

According to the corrected Benesi–Hildebrand formula, the binding constant of the H_2CS sensor and Cu^{2+} was 1.17×10^{11} M^{-1}. In addition, the minimum detection limit (LOD = 5.3×10^{-8} M) and limit of quantity (LOQ = 1.77×10^{-7} M) were also obtained.

pH Effect of the *H_2CS sensor.* In order to study the influence of pH value on H_2CS sensor, H_2CS under different pH conditions was discussed. As depicted in Fig. 9, the fluorescence intensity of the H_2CS sensor has good stability in the pH range 4–14 taking into account the relatively small K_{sp} of $Cu(OH)_2$ (2.2×10^{-20}), coupled with the lower limit of fluorescence (5.3×10^{-8} M); Cu^{2+} below the lower limit will be precipitated as $Cu(OH)_2$ when the pH of the solution is greater than 8. Thus, it is shown that the H_2CS sensor can be used to selectively identify Cu^{2+} in solutions with a pH of 4 to 8.

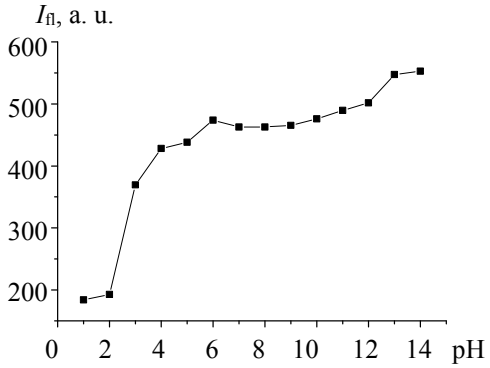

Fig. 9. Changes in fluorescence intensity of H_2CS ($c = 5\times10^{-5}$ M) at different pH values at room temperature (EtOH/H_2O = 1:1, v/v, λ_{ex} = 324 nm, λ_{em} = 374 nm).

Switch response of EDTA. The response of the ultraviolet-visible spectra of the H_2CS switch to EDTA is shown in the Fig. 10a. As Cu^{2+} was added to the ethanol solution of the H_2CS chemical sensor, the absorption band at 290 nm disappeared and a new absorption band appeared at 371 nm. However, when the EDTA solution ($c = 1\times10^{-3}$ M) was added to the solution, we found that the absorption band at 290 nm decreased and the absorption band at 371 nm vanished, and the absorption line returned to the initial position of H_2CS. Then the absorption line returned to the position of H_2CS-Cu^{2+} after addition of Cu^{2+} into the solution again. We performed several experiments and obtained the same results, which show that the H_2CS sensor can be used to continuously identify Cu^{2+}. The fluorescence spectra of Cu^{2+} ions and EDTA added alternately in the H_2CS sensor are shown in Fig. 10b. The results also proved that EDTA can be used as a switch for a sensor to recognize Cu^{2+} ions [52–57]. The logic circuit is shown in Fig. 10c.

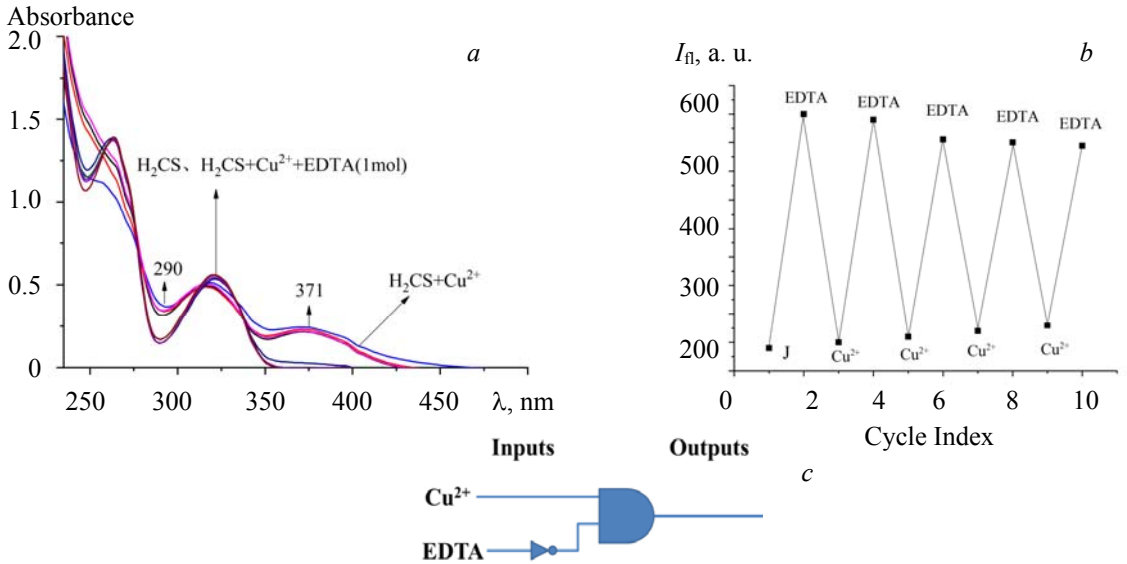

Fig. 10. Detection of reversibility of Cu^{2+} ions by the H_2CS sensor. a) Changes in ultraviolet-visible spectra; b) cycle process of fluorescence spectra; c) switching response.

Time effect of the *H_2CS sensor.* The effect of time on the fluorescence intensity of the H_2CS sensor in EtOH/H_2O (1:1, v/v) solution was also investigated. As can be seen from Fig. 11, the fluorescence intensity of the H_2CS sensor hardly varies with the reaction time.

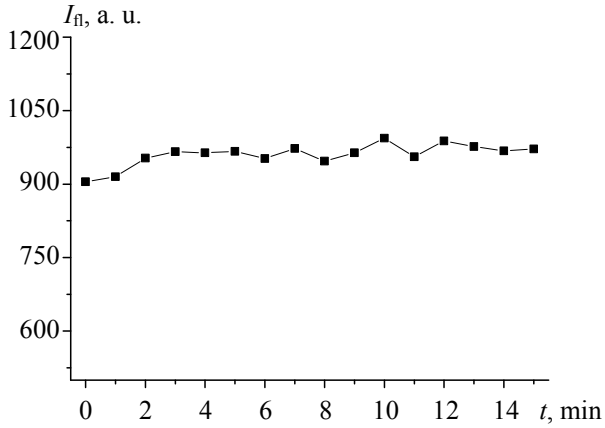

Fig. 11. The time influences of the fluorescent intensity of the H_2CS sensor in EtOH/H_2O (1:1, v/v) solutions.

Temperature effect on recognition. High sensitivity and temperature stability were two important indicators in measuring the practical application value of the H_2CS sensor. In order to better explain the influence of temperature on the sensor, the effect of different temperatures (25, 30, 35, 40, 45, 50, 55, 60, 65, 70, 75, 85, and 90°C) on the sensor were measured. As depicted in Fig. 12, the fluorescence increased gradually with growth in temperature. These phenomena also supported the formation of Cu(II) complex since the higher temperature resulted in the dissociation of weakly bound complexes.

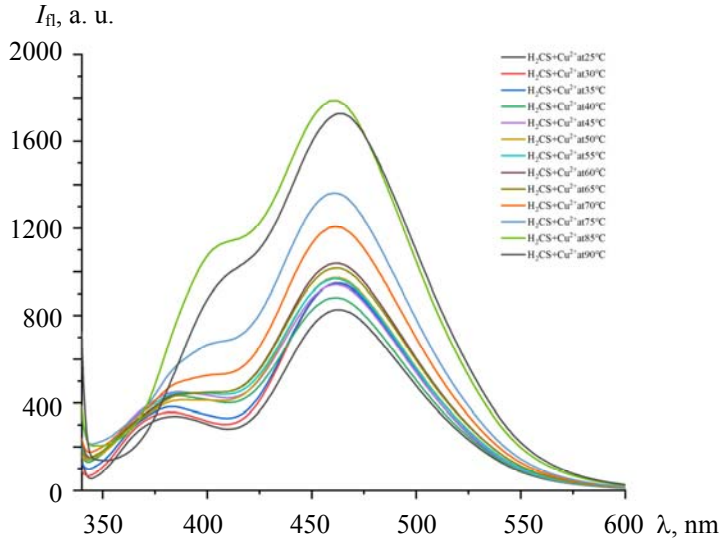

Fig. 12. The fluorescence changes of H_2CS-Cu^{2+} (1:1, 1 μM) at different temperatures.

Practical application on test strips. A paper strip test was performed as described previously to illustrate its practical utility [58], as shown in Fig. 13. Filter paper strips were put into a DMSO (pH 7.4) solution of H_2CS for 5 min and dried with paper, and then put into Cu^{2+} aqueous solution in succession and dried again with paper. Obvious color changes were observed in this process under both visible light and UV irradiation, both of which indicate that the H_2CS sensor has the potential for naked-eye detection of Cu^{2+}.

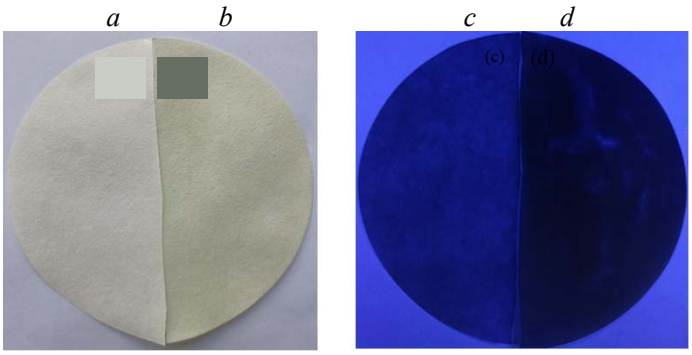

Fig. 13. Color changes on test paper in DMSO (pH 7.4) of a) H_2CS and b) H_2CS-Cu^{2+} under visible light and c) H_2CS and d) H_2CS-Cu^{2+} under UV light.

Conclusions. Symmetric salamo-like small molecule sensor was used to selectively identify Cu^{2+} through two channels. The ion binding properties were studied by UV-vis and fluorescence spectra, which showed that the H_2CS sensor has high sensitivity and selectivity to Cu^{2+} ions. Moreover, the H_2CS sensor shows a 1:1 binging stoichiometry to Cu^{2+} ions with a complexation constant, and the detection limit for Cu^{2+} was also calculated. At the same time, the H_2CS sensor can be used for rapid detection of Cu^{2+} in the basic pH range, which is of great practical value for the detection of Cu^{2+} with the addition of EDTA to realize the cyclic use of sensor molecules.

Acknowledgements. This work was supported by the National Natural Science Foundation of China (21761018) and Overseas Visiting and Research Project for Outstanding Young Talents of Colleges and Universities (gxgwfx2019043), which is gratefully acknowledged.

REFERENCES

1. A. B. More, S. Mula, S. Thakare, S. Chakraborty, A. K. Ray, N. Sekar, S. Chattopadhyay, *J. Lumin*., **190**, 476–484 (2017).
2. A. Zetzsche, N. Schunter, J. Zentek, R. Pieper, *J. Trace. Elem. Med. Biol*., **35**, 1–6 (2016).
3. X. Xu, Y. J. Li, T. Feng, W. K. Dong, Y. J. Ding, *J. Lumin.*, **36**, 169–179 (2021).
4. Q. P. Kang, X. Y. Li, L. Wang, Y. Zhang, W. K. Dong, *Appl. Organomet. Chem.*, **33**, e5013 (2019).
5. J. R. Zimmerman, C. Criss, S. Evans, M. Ernst, M. Nieszala, A. Stafford, J. Szczerba, *Tetrahedron Lett*., **59**, 2473–2476 (2018).
6. L. Z. Liu, L. Wang, M. Yu, Q. Zhao, Y. Zhang, Y. X. Sun, W. K. Dong, *Spectrochim. Acta A*, **222**, 117209 (2019).
7. M. Panchal, M. Athar, P. C. Jhac, A. Kongor, V. Mehta, V. Jain, *J. Lumin.*, **192**, 256–262 (2017).
8. X. Y. Li, Q. P. Kang, C. Liu, Y. Zhang, W. K. Dong, *New J. Chem.*, **43**, 4605–4619 (2019).
9. R. Goel, S. Sharma, K. Paul, V. Luxami, *Sens. Actuators B*, **246**, 776–782 (2017).
10. A. Singh, G. Ramanathan, *J. Lumin.*, **182**, 220–225 (2017).
11. S. Daly, G. Knight, M. A. Halim, A. C. M. Kulesza, F. Choi, P. Chirot, *J. Am. Soc. Mass Spectrom.*, **28**, 38–49 (2017).
12. J. Chang, S. Z. Zhang, Y. Wu, H. Z. Zhang, Y. X. Sun, *Transit. Met. Chem*., **45**, 279–293 (2020).
13. L. Wang, Z. L. Wei, Z. Z. Chen, C. Liu, W. K. Dong, Y. J. Ding, *Microchem. J.*, **155**, 104801 (2020).
14. R. Nakamoto, Y. Nakamoto, T. Ishimori, Y. Fushimi, A. Kido, K. Togashi, *J. Nucl. Med.*, **59**, 846–851 (2017).
15. A. K. Manna, J. Mondal, K. Rout, G. K. Patra, *Sens. Actuators B*, **275**, 350–358 (2018).
16. R. N. Bian, J. F. Wang, Y. J. Li, Y. Zhang, W. K. Dong, *J. Photochem. Photobiol. A*, **400**, 112719 (2020).
17. X. Xu, R. N. Bian, S. Z. Guo, W. K. Dong, Y. J. Ding, *Inorg. Chim. Acta*, **513**, 119945 (2020).
18. A. K. Mahapatra, G. Hazra, N. K. Das, *Sens. Actuators B*, **156**, 456–462 (2014).
19. S. Sumriddetkajorn, K. Chaitavon, Y. Intarvanne, *Sens. Actuators B*, **182**, 592–597 (2013).
20. C. Liu, Z. L. Wei, H. R. Mu, W. K. Dong, Y. J. Ding, *J. Photochem. Photobiol. A*, **397**, 112569 (2020).

21. K. Kise, Y. Hong, N. Fukui, D. Shimizu, D. Kim, A. Osuka, *Mech. J. Chem. Eur.*, **24**, 8306–8310 (2018).
22. M. H. Lee, J. S. Kim, J. L. Sessler, *Chem. Soc. Rev*., **13**, 4185–4191 (2015).
23. S. Z. Zhang, J. Chang, H. J. Zhang, Y. X. Sun, Y. Wu, Y. B. Wang, *Chin. J. Inorg. Chem*., **36**, 503–514 (2020).
24. Y. Zhang, M. Yu, Y. Q. Pan, Y. Zhang, L. Xu, W. K. Dong, *Appl. Organomet. Chem*., **34**, e5442 (2020).
25. K. Ponnuvel, G. Banuppriya, V. Padmini, *Sens. Actuators B*, **234**, 34–45 (2016).
26. Y. Q. Pan, X. Xu, Y. Zhang, Y. Zhang, W. K. Dong, *Spectrochim. Acta A*, **229**, 117927 (2020).
27. R. R. Islangulov, D. V. Kozlov, F. N. Castellano, *Chem. Commun*., **30**, 3776–3778 (2005).
28. C. Liu, X. X. An, Y. F. Cui, K. F. Xie, W. K. Dong, *Appl. Organomet. Chem*., **34**, e5272 (2020).
29. S. K. Sahoo, D. Sharma, A. Moirangthem, A. Kuba, R. Thomas, R. Kumar, A. Kuwar, H. J. Choi, A. Basu, *J. Lumin*., **172**, 297–303 (2016).
30. Y. Q. Pan, Y. Zhang, M. Yu, Y. Zhang, L. Wang, *Appl. Organomet. Chem*., **34**, e5441 (2020).
31. Z. L. Wei, L. Wang, J. F. Wang, W. T. Guo, Y. Zhang, W. K. Dong, *Spectrochim. Acta A*, **228**, 117775 (2020).
32. Y. Upadhyay, S. Bothra, R. Kumar, S. K. Sahoo, *Anal. Chem. Select*., **3**, 6892–6896 (2018).
33. Y. Zhang, L. Z. Liu, Y. D. Peng, N. Li, W. K. Dong, *Transit. Met. Chem*., **44**, 627–639 (2019).
34. L. W. Zhang, Y. Zhang, Y. F. Cui, M. Yu, W. K. Dong, *Inorg. Chim. Acta*, **506**, 119534 (2020).
35. J. B. George, *Inorg. Chim. Acta*, **393**, 135–141 (2012).
36. Y. X. Sun, Y. Q. Pan, X. Xu, Y. Zhang, *Crystals*, **9**, 607 (2019).
37. S. Kine, T. Tadokoro, T. Nabeshima, *Inorg. Chem*., **51**, 11478–11486 (2012).
38. X. X. An, Q. Zhao, H. R. Mu, W. K. Dong, *Crystals*, **9**, 101 (2019).
39. L. Z. Liu, M. Yu, X. Y. Li, Q. P. Kang, W. K. Dong, *Chin. J. Inorg. Chem.*, **35**, 1283–1294 (2019).
40. R. N. Bian, J. F. Wang, Y. J. Li, Y. Zhang, W. K. Dong, *J. Photochem. Photobiol. A*, **400**, 112719 (2020).
41. Q. P. Kang, X. Y. Li, Z. L. Wei, Y. Zhang, W. K. Dong, *Polyhedron*, **165**, 38–50 (2019).
42. H. R. Mu, X. X. An, C. Liu, Y. Zhang, W. K. Dong, *J. Struct. Chem*., **61**, 1218–1229 (2020).
43. X. X. An, Z. Z. Chen, H. R. Mu, L. Zhao, *Inorg. Chim. Acta*, **511**, 119823 (2020).
44. M. Yu, Y. Zhang, Y. Q. Pan, L. Wang, *Inorg. Chim. Acta*, **509**, 119701 (2020).
45. A. G. Jadhav, S. N. Kothavale, *Dyes Pigm*., **138**, 56–67 (2017).
46. J. H. Hu, Y. Sun, J. Qi, Q. Li, T. B. Wei, *Spectrochim. Acta A*, **175**, 125–133 (2017).
47. L. Wang, Z. L. Wei, C. Liu, W. K. Dong, J. X. Ru, *Spectrochim. Acta A*, **239**, 118496 (2020).
48. S. Z. Zhang, G. Guo, W. M. Ding, J. Li, Y. W, H. J. Zhang, J. Q. Guo, Y. X. Sun, *J. Mol. Struct.*, **20**, 129627 (2020).
49. Y. Upadhyaya, T. Ananda, L. T. Babub, P. Pairab, A. K. Skc, R. Kumara, S. K. Sahoo, *J. Photochem. Photobiol. A*, **361**, 34–40 (2018).
50. M. Yu, H. R. Mu, L. Z. Liu, N. Li, Y. Bai, X. Y. Dong, *Chin. J. Inorg. Chem*., **35**, 1109–1120 (2019).
51. T. Anand, S. K. Sahoo, *Phys. Chem. Chem. Phys*., **22**, 11839–11845 (2019).
52. Z. Z. Chen, W. Z. Zhang, T. Zhang, Y. Zhang, W. K. Dong, *New J. Chem*., **44**, 19836–19849 (2020).
53. X. X. An, C. Liu, Z. Z. Chen, K. F. Xie, Y. Zhang, *Crystals*, **9**, 602 (2019).
54. Y. S. Borghei, M. Hosseini, M. R. Ganjali, *Sens. Actuators B*, **273**, 1618–1626 (2018).
55. Q. Zhao, X. X. An, L. Z. Liu, W. K. Dong, *Inorg. Chim. Acta*, **490**, 6–15 (2019).
56. H. R. Mu, M. Yu, L. Wang, Y. Zhang, Y. J. Ding, *Phosphorus, Sulfur, Silicon Rel. Elem*., **195**, 730–739 (2020).
57. S. T. Zhang, P. P. Li, C. Y. Liao, *Spectrochim. Acta A*, **201**, 161–169 (2018).
58. A. Roy, S. Dey, P. Roy, *Sensors Actuators B*, **237** 628–642 (2016).